Electrochimica Acta 258 (2017) 396–404

Contents lists available at ScienceDirect

Electrochimica Acta

journal homepage: www.elsevier.com/locate/electacta

ZnO-based dye-sensitized solar cells: Effects of redox couple and dye aggregation

Esdras J. Canto-Aguilar [a], Manuel Rodríguez-Pérez [a, b, c], Rodrigo García-Rodríguez [a], Francisco I. Lizama-Tzec [a], Alexandra T. De Denko [b], Frank E. Osterloh [b], Gerko Oskam [a, *]

[a] Department of Applied Physics, CINVESTAV-IPN, Mérida, Yucatán 97310, Mexico
[b] Department of Chemistry, University of California - Davis, Davis, CA 95616, USA
[c] Facultad de Ingeniería, Universidad Autónoma de Campeche, Campus V, Colonia Ex Hacienda Kála, C.P.24085, San Francisco de Campeche, Mexico

ARTICLE INFO

Article history:
Received 4 August 2017
Received in revised form
6 November 2017
Accepted 12 November 2017
Available online 13 November 2017

Keywords:
Dye-sensitized solar cells
ZnO
Electrodeposition
Redox chemistry
Solar energy conversion

ABSTRACT

The performance of ZnO-based dye-sensitized solar cells (DSSCs) has always been lower than that of TiO_2-based devices, however, the factors for this difference are still not entirely understood. Here we use current - voltage curves in combination with intensity-modulated photovoltage spectroscopy, charge extraction measurements, and surface photovoltage spectroscopy to gain insight in the photochemical charge separation in ZnO-based DSSCs. Devices were fabricated with electrodeposited nanostructured, mesoporous ZnO films, an organic fluorenyl-thiophene dye (OD-8) as sensitizer, and an electrolyte solution with either the I^-/I_3^- or $[Co(2,2'\text{-bipyridyl})_3]^{2+/3+}$ redox couple. Surface photovoltage measurements and scanning electron microscopy images show that Zn^{2+}-dye aggregates are most likely the cause of a decrease in cell performance with sensitization times longer than 4 h, due to the relatively acidic acrylonitrile bonding moiety of the OD-8 dye. Charge extraction measurements combined with intensity-modulated photovoltage spectroscopy illustrate that a lower electron lifetime for the DSSCs with the $[Co(2,2'\text{-bipyridyl})_3]^{2+/3+}$ redox couple prevents achieving the thermodynamically attainable photovoltage, thus limiting solar cell efficiency. It can be concluded that further improvements in ZnO-based DSSCs are possible by: (i) avoiding the formation of Zn^{2+}-dye aggregates in the mesoporous structure; (ii) preventing back electron transfer from ZnO to the electron acceptor in the electrolyte solution.

1. Introduction

The dye-sensitized solar cell (DSSC) is a fascinating system, where solar cell performance is determined by an optimization of the electrical properties of nanomaterials, optical properties of molecular sensitizers, and redox properties of a non-aqueous electrolyte solution. If both light absorption by the sensitizer and electron injection into the nanostructured metal oxide film are efficient, then the key to good performance is a high electron collection efficiency. This is determined by the relative rates of electron transport in the nanostructured film and the electron transfer rates to the oxidized dye or the electron acceptor in the solution, which are the two main recombination processes. After the groundbreaking work reported in 1991, when the first device with a power conversion efficiency above 7% was reported [1], subsequent work has focused on improving the solar absorptance by engineering the dye chemistry [2] and optimizing the I^-/I_3^- electrolyte solution, leading to an 11.1% confirmed solar cell efficiency in 2006 [3]. Further improvements in the efficiency were achieved by changing the redox couple, based on the observation that a more positive redox potential could lead to a higher cell voltage [4]; the combined use of new organic dyes with cobalt-based redox couples resulted in cells with an efficiency of more than 13% in 2014 [5–7]. Recently, an efficiency of more than 14% has been reported [8], although the cell design of these high-efficiency cells are not yet suitable for scale-up. Alongside the development of higher efficiency solar cells, a better understanding of the electronic transport and recombination processes in the solar cell has been obtained [5,6,9–12].

Traditionally, nanostructured, mesoporous TiO_2 is used for efficient DSSCs, however, ZnO is an interesting alternative as an n-

* Corresponding author.
E-mail address: gerko.oskam@cinvestav.mx (G. Oskam).

https://doi.org/10.1016/j.electacta.2017.11.075
0013-4686/

type material with direct electronic transitions with similar band gap (3.3 eV, versus 3.2 eV for anatase TiO_2), and a higher bulk electron mobility (200 $cm^2\ V^{-1}\ s^{-1}$ versus 0.1–4 $cm^2\ V^{-1}\ s^{-1}$ for TiO_2) [13]. In addition, ZnO can be obtained by various techniques such as sol-gel [14,15], precipitation [16–18], hydrothermal synthesis [19,20] and electrochemical methods; in particular, electrodeposition is an attractive technique due to its high deposition speed, good control over thickness and morphology of the film, as well as low temperature deposition conditions [21–29]. The better electrical properties of ZnO are attractive in order to better compete with recombination; however, the record efficiency for ZnO is 8.0%, compared to 14% for TiO_2 [30]: in specific systems, it has been shown that this may be related to a slower electron injection rate [31], faster electron transfer to the electrolyte solution, and less than optimal interaction of the dye with the ZnO surface, resulting in partial dissolution of ZnO but also lower dye coverage [32]. ZnO is not as stable as TiO_2 in acidic solutions, which is specifically problematic when using classical dyes designed for TiO_2 that use a carboxylic acid moiety as anchoring group: during the sensitization step, the ZnO surface is attacked leading to the formation of Zn^{2+}-dye aggregates, resulting in pore blocking and lower electron injection [13]. We believe that the use of appropriate dyes and redox couples can improve the efficiency of ZnO-based dye-sensitized solar cells.

In this work, we aim to explore some of the factors that limit the efficiency of ZnO-based DSSCs. Nanostructured, mesoporous ZnO films were electrodeposited from an optimized aqueous $ZnCl_2$ solution. DSSCs were assembled using an organic fluorenyl-thiophene dye (OD-8), and electrolyte solutions with either the I^-/I_3^- or the cobalt complex based $[Co(2,2'\text{-bipyridyl})_3]^{2+/3+}$ redox couple. By combining the results from standard current - voltage measurements, small-signal perturbation techniques, and surface photovoltage spectroscopy, it is concluded that the efficiency of ZnO-based DSSCs is limited by recombination via electron transfer to the electron acceptor in solution and the formation of Zn^{+2}-dye aggregates.

2. Experimental

2.1. Chemicals

$ZnCl_2$ (Sigma-Aldrich; ≥ 98%), KCl (Sigma-Aldrich, ≥ 99%), cetyltrimethylammonium bromide, (CTAB; Sigma-Aldrich, 98%), Co(II) tris(bipyridyl) tetracyanoborate (Co-200; Eversolar, 98%), Co(III) tris(bipyridyl) tetracyanoborate (Co-300; Eversolar, 98%), 1,2-dimethyl-3-propylimidazolium iodide (DMPII, IonLic DMPII; Solaronix), Chenodeoxycholic acid (CDCA; Sigma-Aldrich, ≥97%), Polyvinylpyrrolidone (PVP40; Sigma-Aldrich), t-Butyl alcohol (Sigma-Aldrich, ACS ≥99%), ethanol anhydrous (J.T Baker, 99%), Methanol (Sigma-Aldrich, 99.8%), Acetonitrile (Sigma-Aldrich, 99.93%), 4-tert-Butylpyridine (Sigma-Aldrich, 96%), H_2SO_4 (Sigma-Aldrich, 98%), HCl (Sigma-Aldrich, 37%), Oxygen (Praxair, 99.5%), Platisol T (Solaronix), Metlonix 1170-60 (Surlyn 60 μm thick, Solaronix), and Water (18 MΩ cm resistivity). All solvents and chemicals were used in ambient conditions (room temperature and atmospheric pressure), and without further purification.

2.2. Preparation of electrodeposited ZnO films

Porous films of ZnO were obtained through the use of a galvanostatic electrodeposition method using a Gamry Instruments Reference 3000 potentiostat/Galvanostate/ZRA with Ag/AgCl (3 M KCl) as a reference electrode, Pt as a counter electrode and SnO_2:F-coated glass substrate (FTO, TEC 8 Ω sq^{-1}, Pilkington) as a working electrode. A 0.5 cm^2 area was masked with polyester tape (Cole-Parmer), and activated with 2 M H_2SO_4 followed by rinsing with deionized water. The electrolyte was prepared with 0.01 M $ZnCl_2$, 0.1 M KCl and 0.10 mM PVP40. The solution was bubbled with O_2 for 20 min before use. For the electrodeposition a current density of −0.5 mA cm^{-2} was applied for 8427.12 s. All the films were sintered at 450 °C for 1 h after electrodeposition.

2.3. Preparation of dye solutions and sensitizing of ZnO films

The dye used in this work was the (Z)-2-Cyano-3-(5-(9,9-dihexyl-7-(dihexylamino)-9H-fluoren-2-yl)thiophen-2-yl)acrylic acid (*OD-8;* from *Eversolar*); 0.5 mM OD-8 and 0.5 mM CDCA solutions were prepared to dissolve the desired amounts of these reagents in a mixture of acetonitrile/t-butyl alcohol (1:1 v/v). ZnO films were heated at 90 °C for 20 min and immediately soaked in the dye solution (described above) for different times (1, 4, 8 and 24 h) in order to achieve sensitization. After sensitization, the films were removed from the dye solution and carefully washed with the same mixture of acetonitrile/t-butyl alcohol.

2.4. Preparation of electrolyte solutions

All the electrolyte solutions used were prepared in a 5 mL volumetric flask using acetonitrile as solvent. The cobalt redox couple consists of 0.22 M $[Co(2,2'\text{-bpy})_3]^{2+}$ (0.8329 g), 0.05 M $[Co(2,2'\text{-bpy})_3]^{3+}$ (0.218 g) and 0.2 M 4-tert-butylpyridine (0.1352 g). The I^-/I_3^- redox couple was prepared in the same molar ratio as for the Co-based redox couple, using 0.05 M iodine (0.0634 g), 0.2 M TBP, and 0.27 M 1,2-dimethyl-3-propylimidazolium iodide (0.3592 g). The chemical structures of all the redox couples, dyes, CDCA and PVP40 are shown in the Supporting Information (Fig. S1).

2.5. Electrochemical characterization of solutions

The electrochemical spectrum of the working solutions was obtained by performing cyclic voltammetry with a potentiostat/galvanostat/ZRA (Gamry Instruments Reference 3000) employing a classic three-electrode system with as a reference electrode a Ag/AgCl (3 M KCl) for aqueous solution and a Ag/Ag^+ (0.01 M $AgNO_3$) for organic solutions, a Pt counter electrode and an FTO (TEC 8), Pt or Au working electrode depending on the system studied. Rotating disc electrode (RDE) procedures with the same three-electrode configuration were carried out to determine the diffusion coefficient of the electroactive species in the electrolyte solutions. The rotation rates of the Au or Pt disk were controlled with a Radiometer Analytical CTV101 speed control system.

2.6. Preparation and photovoltaic characterization of DSSC

Dye-sensitized solar cells (DSSCs) were prepared with the sensitized ZnO films described previously and an FTO counter electrode with a thin coating of Pt, prepared by spreading a drop of Platisol (Solaronix) on the conductive side of the electrode and subsequent heating at 450 °C for 5 min. The photoanode and counter electrode were sealed in a sandwich configuration using a Surlyn (60 μm) separator by heating at 210 °C for 2.5 min. Finally, the electrolyte solution was introduced inside the cell through a pair of holes previously perforated in the counter electrode, which were subsequently sealed with Surlyn and a microscope cover glass pressed under heating. Photovoltaic characterization was performed using a set-up consisting of a 450 W ozone-free Xe-lamp (Newport Corporation) with a water filter, calibrated to an irradiance of 100 mW cm^{-2} on the surface of the solar cell using an Air Mass 1.5 Global (AM 1.5G) optical filter (Newport Corporation). The

intensity was calibrated using a certified 4 cm^2 monocrystalline silicon reference cell with incorporated KG-5 filter. Current–voltage curves (I–V), intensity modulated photovoltage spectroscopy (IMVS) and charge extraction measurements were recorded with an Autolab PGSTAT302 N/FRA2 set-up (Metrohm Autolab). In charge extraction measurements, the dye-sensitized solar cells were illuminated under open circuit conditions until a steady photovoltage was obtained. The illumination was then switched off and the cell was switched to short circuit conditions where the resulting current collected for 90 s was integrated; this integrated current corresponds to the electronic charge accumulated in the film. In the IMVS technique, a sinusoidal, small amplitude light perturbation at different frequencies superimposed on a bias light intensity is applied to the DSSC under open circuit conditions. The transfer function between the modulated light intensity and the measured AC potential of the cell provides information on the electronic lifetime under open circuit conditions. IMVS measurements were performed at modulation frequencies between 1 mHz and 10 kHz. A red LED (625 nm) was used to illuminate the sample from the substrate side and it served both as the bias illumination and the small sinusoidally modulated probe beam.

The crystal phase and texture of ZnO materials were analysed with a Siemens D-5000 difractometer with Cu-Kα radiation at 34 kV and 25 mA; the diffraction patterns were collected from 10° to 70° (2θ) with a 0.02° step size and 2 s integration time, with the films at a 3° inclination. SEM measurements were carried out using a scanning electron microscope (JEOL JSM 7600 F) operated at an accelerating voltage of 15 kV, and using the SEI detector. The thickness of the films was determined using a KLA Tencor D-120 profilometer. Diffuse reflectance spectra were recorded on films using a Thermo Scientific Evolution 220 UV–Vis spectrometer.

Surface photovoltage (SPV) measurements were conducted under vacuum (1.6×10^{-4} mBar) on ZnO films on FTO. A gold Kelvin probe (Delta PHI Besocke) served as the reference electrode. Samples were illuminated with monochromatic light from a 150 W Xe lamp filtered through an Oriel Cornerstone 130 monochromator with light intensity range of 0.1–0.3 mW cm^{-2}. The CPD spectra were corrected for drift effects by subtracting a dark scan. No correction for the variable light intensity from the Xe lamp was performed. Samples for SPS measurements were prepared by heating FTO/ZnO substrates at 310 °C for 20 min followed by cooling to 80 °C and followed by placement into the dye solutions for 1 h to 24 h. After sensitization, all films were rinsed with a mixture of acetonitrile/t-butyl alcohol (1:1 v/v), and stored in aluminum foil covered containers in the glovebox.

3. Results and discussion

3.1. Electrochemical deposition of ZnO

Methods to electrodeposit ZnO from aqueous solutions can be divided into two groups: (i) reduction of a zinc salt solution to metallic zinc and simultaneous and subsequent oxidation of the metallic zinc using dissolved oxygen to form ZnO, and (ii) reduction of a different component of the zinc salt solution, such as nitrate, to form a large concentration of surface hydroxide resulting in deposition of $Zn(OH)_2$ and subsequent condensation to ZnO. Experimental parameters, including concentration of the solution components, pH of the solution, temperature, deposition current or potential, either pulsed or steady-state, etc. can be used to control the composition and morphology of the final product [23,33].

Fig. 1 shows two current - potential curves for an FTO (fluorine-doped tin oxide) working electrode and a solution containing $ZnCl_2$ + KCl at neutral pH, which was saturated with either N_2 or O_2 in order to determine the reaction mechanism leading to

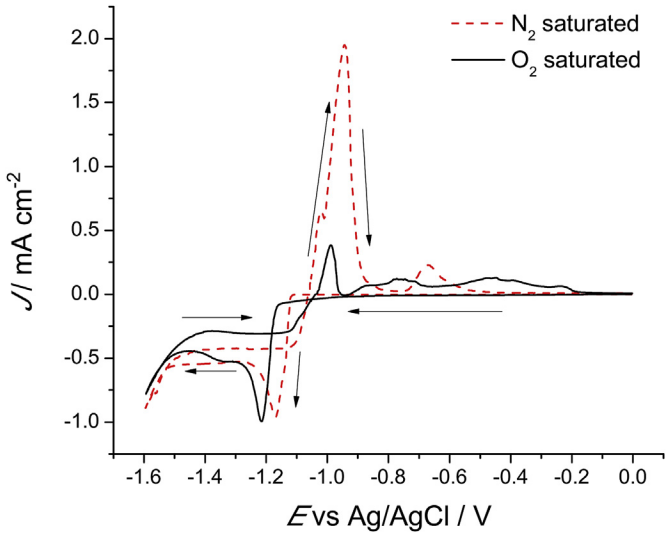

Fig. 1. Current-potential curves obtained in a solution of 0.01 M $ZnCl_2$ + 0.10 M KCl using an FTO-TEC8 working electrode after either O_2 or N_2 bubbling for 20 min. The experiments were performed at room temperature (25 °C) and at a scan rate of 2 mV s^{-1}.

electrodeposition of ZnO. Both N_2 and O_2 bubbled solutions showed a cathodic current maximum at around −1.16 and −1.21 V, respectively, related to the reduction of Zn^{2+} and nucleation and growth of mainly metallic Zn. The electrochemical reduction of O_2 is expected to also take place in this potential range; however, the associated current is relatively low. At more negative potentials (−1.5 V vs Ag/AgCl) water reduction becomes the main electrochemical reaction. When reversing the direction of the potential sweep, an anodic current maximum is observed in both systems at −0.94 and −0.98 V, respectively, which corresponds to the electrochemical oxidation of the metallic zinc previously deposited. The anodic peak is significantly smaller for the solution saturated with oxygen, and this observation can be understood in the framework of mechanism (i). Even during the cathodic sweep, electrodeposited metallic Zn reacts with the oxygen dissolved in the solution forming ZnO. Hence, upon reversing the sweep towards positive potentials, only traces of metallic zinc are present, resulting in a small electrochemical oxidation peak. In the solution saturated with nitrogen, most metallic zinc remains and is electrochemically oxidized upon sweeping the potential towards positive potentials resulting in a large oxidation peak.

In order to better control the morphology and porosity of the ZnO films, the water-soluble polymer PVP40 (polyvinylpyrrolidone; M_W = 40,000 g mol^{-1}) was added to the solution. Current - potential curves (see Supporting Information, Fig. S2) illustrate that PVP40 is not electrochemically active and does not markedly change the electrochemical behavior of the deposition bath.

Fig. 2 shows X-ray diffraction patterns of the films electrodeposited from O_2-saturated 0.01 M $ZnCl_2$ + 0.10 M KCl with 0.1 mM PVP40 onto FTO before and after sintering at 450 °C. The patterns show that electrodeposition at room temperature results in a crystalline film. Before sintering (Fig. 2a), peaks associated with both metallic zinc and ZnO are observed, as well as reflections related to the FTO substrate; notably, peaks related to $Zn(OH)_2$ are absent, supporting the prevalence of mechanism (i). It should be noted that during the cathodic sweep, water and O_2 may also be reduced, which could lead to an increase in the surface pH, which may affect the composition of the deposited material [23,29]. After sintering in air (Fig. 2b), metallic Zn has been oxidized to ZnO with the hexagonal crystal structure.

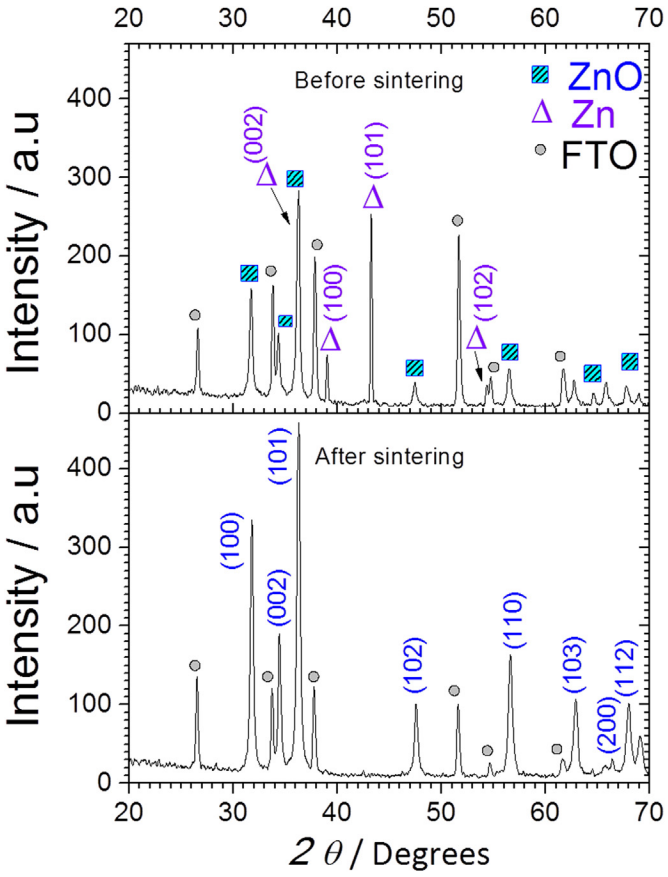

Fig. 2. X-ray diffraction patterns of electrodeposited ZnO films from the O_2-saturated 0.01 M $ZnCl_2$ + 0.10 M KCl with 0.1 mM PVP40 on FTO, (a) before, and (b) after sintering. Before sintering, the (002), (100), (101) and (102) peaks associated with metallic zinc are indicated (JCPDS# 04-0831); after sintering the (100), (002), (101), (102), (110), (103), (200) and (112) reflections corresponding to ZnO (JCPDS# 36-1451) are identified. In both figures, the peaks corresponding to the FTO substrate are also indicated (JCPDS# 41-1445).

The morphology of the sintered ZnO films is shown in Fig. 3. The SEM images illustrate that the film is mainly composed of clusters of rounded particles with sizes between 10 and 50 nm; however, other structures such as thin needles with lengths of up to 1 μm, as well as non-porous agglomerates of about 1 μm, are also observed. The presence of "rounded" particles is associated with the presence of PVP40 in the deposition bath: PVP40 adsorbs at a similar rate on the different faces of the growing ZnO particles, thus modulating grain size and morphology [21]. The presence of needles is characteristic of the preferential nucleation and growth of ZnO by the electrodeposition route [29]. For the fabrication of DSSCs, mesoporous and nanostructured ZnO films with an average thickness of 9.23 ± 0.74 μm were obtained through galvanostatic electrodeposition.

3.2. Electrochemical characterization of redox couples and dye

The redox potential for the electrolyte solutions used in DSSCs was determined through near steady-state voltammetry. Fig. 4a shows the current - potential curves obtained at a very low scan rate of 0.5 mV s^{-1} for the electrolyte solutions used in the solar cells. At conditions close to steady state, the average potential where the current is zero corresponds to the redox potential (E*) of the couple. For the I^-/I_3^- redox couple, the redox potential is located at −0.170 V vs. Ag/Ag^+ while for the $[Co(bpy)_3]^{2+/3+}$ couple the redox potential is 0.014 V vs. Ag/Ag^+. Hence, the $[Co(bpy)_3]^{2+/3+}$ redox potential is 0.184 V more positive than that of the I^-/I_3^- redox couple, which implies that based on thermodynamic grounds a higher open circuit potential could be achieved in the DSSCs [34–36]; however, the open circuit potential may also be limited by the kinetics of the recombination process. Table 1 summarizes the electrochemical properties of the redox couples.

The two redox couples used in the acetonitrile-based electrolyte solution for the dye-sensitized solar cells were characterized using current - potential curves at a rotating disk electrode (RDE) as a function of the rotation rate. Fig. S3 illustrates that the current - potential curves are characterized by current plateaus at sufficiently large overpotential in all cases, and the limiting current density versus the square-root of the angular rotation speed shows a linear behavior through the origin (Fig. S4). The results indicate that the plateau current density is limited by diffusion according to the Levich equation (eq. (1)):

$$I_L = 0.62\, n\, F\, D^{2/3}\, \nu^{-1/6}\, c^{\infty}\, \omega^{1/2} \quad (1)$$

where I_L is the limiting current density (A cm^{-2}), n is the number of electrons involved in the reaction, F is the Faraday constant (C mol^{-1}), D is the diffusion coefficient of the electroactive species (cm^2 s^{-1}), ν is the kinematic viscosity of the solvent (4.484×10^{-3} cm^2 s^{-1} for acetonitrile), c^{∞} is the bulk concentration (mol cm^{-3}), and ω is the angular rotation speed (rad s^{-1}).

The Levich analysis allows us to determine the diffusion coefficients for both the reduced and oxidized species of the $[Co(bpy)_3]^{2+/3+}$ and I^-/I_3^- redox couples. In Table 1, the results are summarized, and it can be observed that the diffusion coefficients for the I^-/I_3^- redox couple are about twice as large as those of the $[Co(bpy)_3]^{2+/3+}$ couple, which is likely related to the larger size of the latter molecules [34,35].

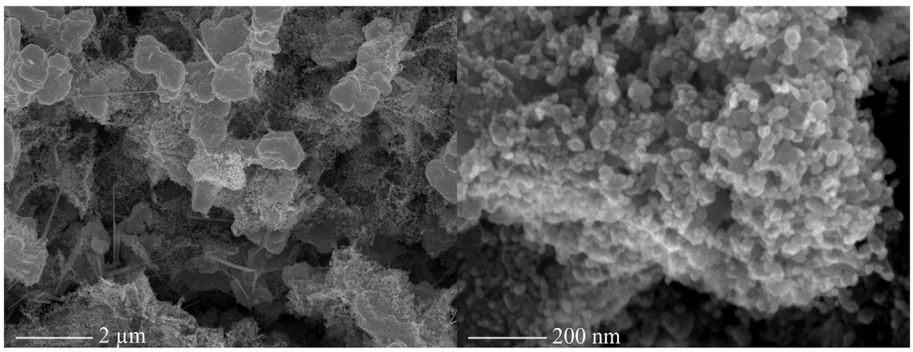

Fig. 3. SEM images of ZnO films sintered at 450 °C and electrodeposited from O_2-saturated 0.01 M $ZnCl_2$ + 0.10 M KCl with 0.1 mM PVP40 onto FTO.

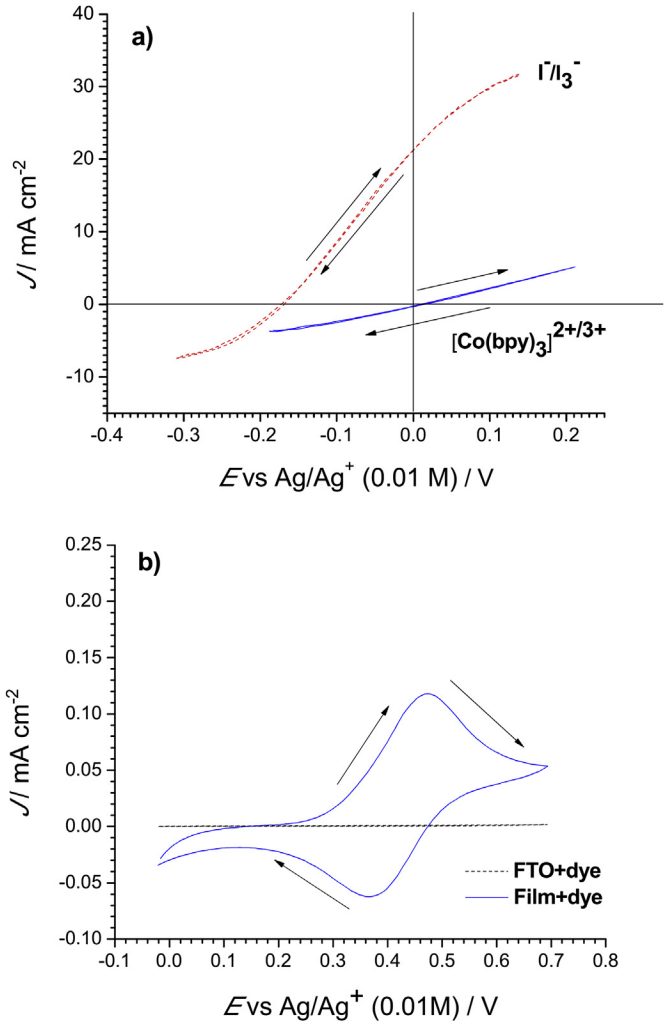

Fig. 4. a) Cyclic voltammetry at a scan rate of 0.5 mV s^{-1} for the DSSC solutions: 0.22 M I^-, 0.05 M I_3^-, 0.2 M TBP in acetonitrile at a Pt electrode (dashed line); 0.22 M $[Co(bpy)_3]^{2+}$, 0.05 M $[Co(bpy)_3]^{3+}$, 0.2 M TBP in acetonitrile at a Au electrode (continuous line); b) Cyclic voltammetry at 50 mV s^{-1} for OD-8 adsorbed onto a nanostructured, mesoporous ZnO film in a 0.1 M $[Bu_4N][PF_6]$ solution. Experiments were performed at 25 °C.

In order to determine the HOMO level of the dye, cyclic voltammetry was carried out for the OD-8 dye in solution and adsorbed onto an electrodeposited ZnO film. For the dye in solution (Fig. S5), the electrochemical characterization was performed using platinum as working and counter electrodes and a 0.5 mM OD-8 + 0.1 M $[Bu_4N][PF_6]$ electrolyte solution in acetonitrile. Oxidation and reduction peaks attributed to the $(OD\text{-}8)^0/(OD\text{-}8)^+$ redox couple are observed at 0.403 V and 0.312 V vs. Ag/Ag^+, respectively. The observation that the cathodic and anodic current maxima are essentially the same in magnitude and that the peak separation is about ≈ 91 mV indicate that the redox reaction is close to reversible. Cyclic voltammetry of dyed ZnO films, prepared using a soaking time of 1.5 h in a 0.5 mM OD-8 + 0.5 mM CDCA solution in acetonitrile/tert-butyl alcohol (1:1 v/v), shown in Fig. 4b, reveals oxidation and reduction peaks at 0.453 and 0.370 V vs. Ag/Ag^+, respectively, with a peak separation of ≈ 83 mV and symmetric oxidation and reduction waves at a scan rate of 50 mV s^{-1}. A slight shift is observed with respect to the values of the oxidation and reduction peaks of the dye in solution; for the dye adsorbed on the ZnO surface, the equilibrium redox potential is 62 mV more positive due to the interaction between ZnO and dye. Table 2 summarizes the electrochemical properties measured for the OD-8 dye.

3.3. Dye sensitized solar cells (DSSCs)

Dye-sensitized solar cells were prepared using electrodeposited nanostructured, mesoporous ZnO films with a thickness of 9.23 ± 0.74 μm, the OD-8 dye, and both redox couples. Fig. 5a presents a set of current - voltage curves for DSSCs using the $[Co(bpy)_3]^{2+/3+}$ redox couple as a function of the immersion time of the ZnO films in the sensitizing OD-8 solution. The results are summarized in Table 3.

The progressive increase of the short circuit current density (J_{SC}) up to 4 h immersion time is related with the gradual increase of the number of dye molecules adsorbed to the ZnO surface (Fig. 6a and c). However, at longer immersion times J_{SC} decreases significantly, which can be interpreted in terms of the reported limited stability of ZnO in acidic media. Since the OD-8 dye has a carboxylic acid moiety as anchoring group, the dye solution is somewhat acidic, and ZnO has been known to partially dissolve and form Zn^{2+}-dye aggregates, which may block the pores in the nanostructure [37–40]. Although the aggregates are difficult to observe with SEM, the ZnO surface tends to become smoother with longer immersion times, which may be related to selective dissolution of ZnO material that can be incorporated in aggregates (see Fig. S6 in the Supporting Information). The Zn^{2+}-dye aggregates may provide optical absorption, explaining the "colorful" appearance of the film, however, generally electron injection into the ZnO conduction band does not occur from these aggregates. This interpretation is confirmed by surface photovoltage spectroscopy in combination with optical reflectance measurements on dye-sensitized ZnO films at different sensitization times of 1 h and 24 h. In Fig. S7 in the Supporting Information, it can be seen that there is more dye present in the mesoporous ZnO film after 24 h, illustrated by the more intense band at 2.7 eV (459 nm) in the optical spectrum, however, the contact potential difference (CPD) at that energy is in fact

Table 2
Data obtained from cyclic voltammetry for the dye in solution and adsorbed on ZnO films.

	OD-8 in solution	OD-8 adsorbed onto ZnO
E_{ox} vs Ag/Ag^+/ V	0.405	0.469
E_{red} vs Ag/Ag^+/ V	0.312	0.373
E° vs Ag/Ag^+/ V	0.359	0.421
E° vs NHE/ V	0.899	0.961
E_{HOMO} / eV (estimated)	−5.399	−5.461

Table 1
Diffusion coefficients and redox potentials determined by electrochemical techniques.

Electroactive species	D / cm^2 s^{-1}	Redox reaction	E^* vs Ag/Ag^+/ V	E^* vs NHE/ V
I_3^-	1.8×10^{-5}	$I_3^- + 2e^- \rightarrow 3I^-$	−0.170	0.370
I^-	1.9×10^{-5}			
$[Co(bpy)_3]^{3+}$	8.7×10^{-6}	$[Co(bpy)_3]^{3+} + e^- \rightarrow [Co(bpy)_3]^{2+}$	0.014	0.554
$[Co(bpy)_3]^{2+}$	9.2×10^{-6}			

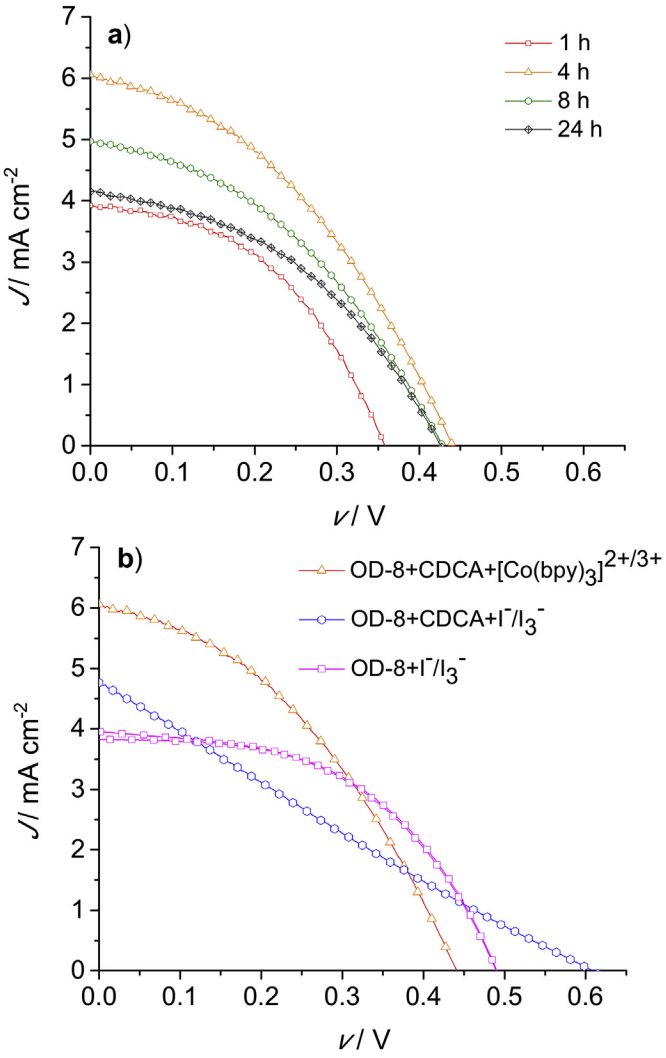

Fig. 5. a) Current density - voltage curves for electrodeposited ZnO-based DSSCs with the organic dye OD-8 and $[Co(bpy)_3]^{2+/3+}$ redox couple as a function of sensitization time; b) Current density - voltage curves for electrodeposited ZnO-based DSSCs with the organic dye OD-8 sensitized for 4 h, for the two different redox couples used; in addition, a current-voltage curve for a DSSC with the I^-/I_3^- redox couple and a ZnO film sensitized for 2 h in a OD-8 dye solution without CDCA is presented.

somewhat smaller than for the 1 h sample. Hence, in agreement with the desorption measurements, there is more dye present after 24 h, but the injection efficiency appears lower, resulting in a smaller *CPD* signal; in addition, the spectrum presents more noise for the 24 h sample, which is an indication of the presence of aggregates. Note that the lower injection efficiency is in agreement with the observation that the short circuit photocurrent is smaller for DSSC after 24 h of sensitization.

Fig. 5b shows the current - voltage curves for DSSCs prepared with the optimal 4 h immersion time for both redox couples. A pronounced difference in the fill factor (*FF*) is observed: the I^-/I_3^- solar cell prepared using the co-adsorbent CDCA in the sensitization process has a much lower *FF* than the corresponding solar cell with the $[Co(bpy)_3]^{2+/3+}$ redox couple. The electrochemical characterization of the redox couples indicate that the diffusion coefficients for the I^-/I_3^- redox couple are a factor 2 larger than for the $[Co(bpy)_3]^{2+/3+}$ redox couple, hence, one would not expect diffusion of the redox couple in the bulk solution to be a reason for the smaller fill factor for the I^-/I_3^- redox solution. However, transport of the redox couple in the mesoporous film is expected to depend on the interaction between the redox couple and the ZnO surface, the dye and the co-adsorbent; it appears that this combination of interactions causes the lower fill factor for the I^-/I_3^- solar cells. In fact, Fig. 5b shows that if the co-adsorbent CDCA is not used, the classical diode-shaped I–V curve is recovered for the I^-/I_3^- solar cells. However, if CDCA is not used during sensitization, the DSSCs with the $[Co(bpy)_3]^{2+/3+}$ redox couple have a very low efficiency. Hence, for sake of comparison, we used the same sensitization solution chemistry for both redox couples. Note that the results obtained for the separate components using classical electrochemistry do not tell the entire story in this complex system.

The open circuit potential (V_{OC}) on the other hand increases with the immersion time, without showing a reversal in trend (Fig. 6b). This is generally observed for dye-sensitized solar cells (and many other types of solar cells) if the recombination kinetics do not increase markedly with dye coverage: upon increasing the dye coverage, the injection current increases, hence, in order to achieve zero current by balancing the injection with recombination rate, a higher voltage is required. The dependence of recombination rate on voltage thus defines V_{OC}. On the other hand, the recombination rate may actually decrease due to a better surface passivation with increased dye and / or co-adsorbent (CDCA) coverage; this would also lead to an increase in V_{OC} with immersion time. However, since the decrease in J_{SC} is much more pronounced than the increase in V_{OC}, an optimum sensitization time exists for the ZnO - OD-8 system.

Fig. 7 shows a band diagram illustrating the effects of the change in redox potential on the energetics and kinetics of the DSSC: for the same quasi-Fermi level under open circuit conditions corresponding to the FTO/ZnO electrode, assuming the change in redox couple does not lead to a shift of the band edges, the open circuit potential of the DSSC is expected to be 184 mV larger for the $[Co(bpy)_3]^{2+/3+}$ redox couple, but only if: (i) dye regeneration is sufficiently fast, and (ii) recombination of ZnO electrons with the oxidizing agent is sufficiently slow. If dye regeneration is slow due to the smaller driving force for the regeneration process with the $[Co(bpy)_3]^{2+/3+}$ redox couple, then recombination of ZnO electrons with the oxidized dye is expected to limit the open circuit voltage; if recombination of ZnO electrons with the oxidizing agent is fast, then the thermodynamically attainable open circuit potential cannot be maintained, and will be smaller than expected.

However, as can be observed from Fig. 5 and Table 3, the open circuit potential for the cells with the $[Co(bpy)_3]^{2+/3+}$ redox couple was around 140 mV smaller than obtained for I^-/I_3^- solar cells. This can be related with the recombination processes that govern the efficiency of the DSSC.

Table 3
Short circuit current density (J_{SC}), open circuit potential (V_{OC}), fill factor (FF) and efficiency (η) for DSSCs for different sensitization times and redox couples.

Redox couple	Time/ h	J_{SC} / mA cm^{-2}	V_{OC} / V	*FF*	η / %
$[Co(bpy)_3]^{2+/3+}$	1	3.91 ± 0.18	0.34 ± 0.02	0.46 ± 0.01	0.62 ± 0.06
	4	5.87 ± 0.18	0.44 ± 0.01	0.38 ± 0.03	0.97 ± 0.07
	8	5.39 ± 0.4	0.42 ± 0.01	0.4 ± 0.02	0.91 ± 0.11
	24	4.2 ± 0.16	0.41 ± 0.02	0.46 ± 0.05	0.79 ± 0.14
I^-/I_3^-	4	4.47 ± 0.27	0.58 ± 0.03	0.26 ± 0.02	0.66 ± 0.03

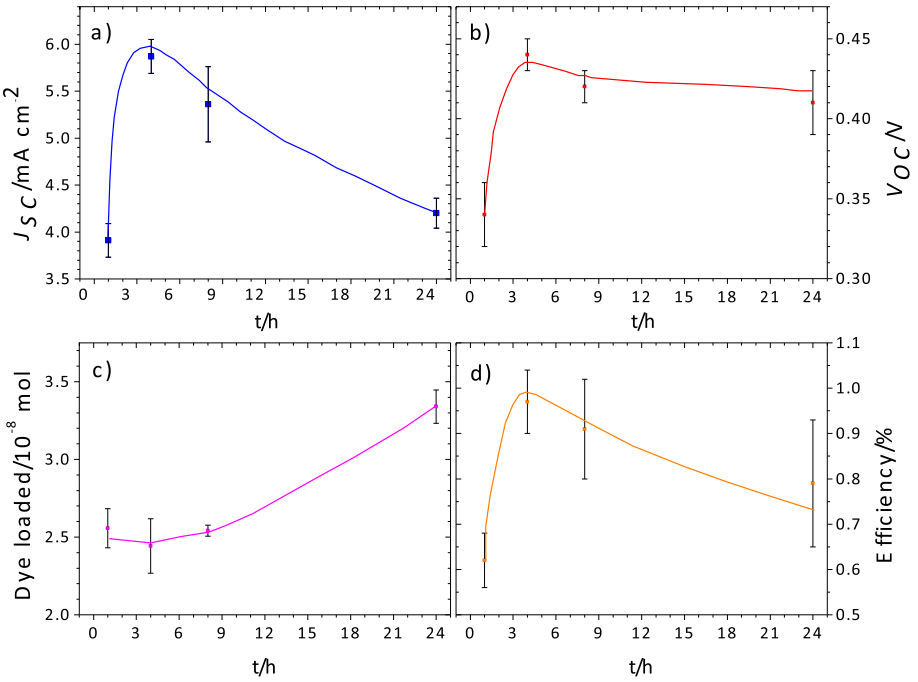

Fig. 6. Evolution of: a) short circuit current density, b) open circuit potential, c) dye loading, and d) efficiency of ZnO-OD-8-$[Co(bpy)_3]^{2+/3+}$ based DSSCs as a function of sensitization time.

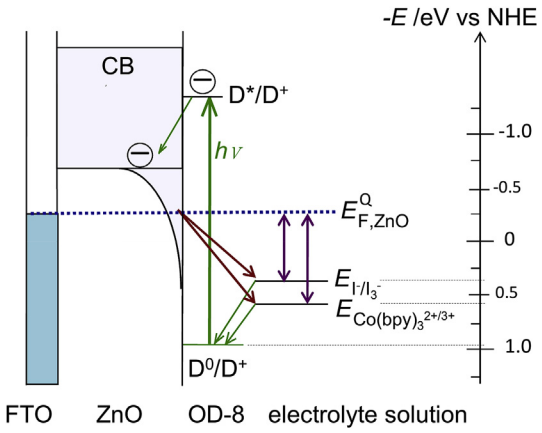

Fig. 7. Schematic band diagram illustrating the effect of the redox potential on the attainable open circuit potential of the DSSC. If the recombination processes are sufficiently slow, then the open circuit potential is expected to be larger for the cells with the $[Co(bpy)_3]^{2+/3+}$ redox couple.

In order to obtain a better insight into these processes, 3 cells of each redox couple were characterized via charge extraction and IMVS measurements. In charge extraction measurements, the cell is held at open circuit under illumination until the system is stable, and then the illumination is switched off and the cell is switched to short circuit simultaneously, and the current transient corresponding to equilibration under dark conditions is integrated to obtain the charge. In IMVS, the cell is held at open circuit under illumination, and a small, sinusoidally modulated light intensity is applied to the cell and the corresponding modulated photovoltage is measured as a function of modulation frequency. In general, a single time constant is measured, corresponding to the electron lifetime. Both experiments are performed as a function of steady-state light intensity. Charge versus voltage curves for the two sets of cells show that the electrodeposited ZnO photoanodes are characterized by an exponential distribution of traps below the conduction band, as has previously been reported for TiO_2 and ZnO-based DSSCs [41], and as schematically illustrated in Fig. 7. The trap distribution parameter obtained from the slope is very similar for both redox couples, indicating that the general dependence of the trap state density with the accumulated charge concentration in the semiconductor is not affected by the redox potential in the electrolyte solution [42]. The electron lifetime is plotted against the total charge extracted in Fig. 8a.

From Fig. 8 it can be observed that the dependence of electron lifetime with charge extracted follows an exponential behavior for all the cells. As can be seen in Fig. 8, at the same charge, corresponding to the same quasi-Fermi level with respect to the ZnO conduction band edge, the electron lifetime is about 70× larger for the cells with the I^-/I_3^- redox couple. In addition, it can be seen that larger values for the charge can be extracted for the cells with the I^-/I_3^- redox couple, indicating that the quasi-Fermi level reached at a certain light intensity is higher than for the $[Co(bpy)_3]^{2+/3+}$ cells; this observation corresponds to the capability to maintain a larger open circuit potential. These results are also observed in Fig. 8b, where the lifetime is plotted against the cell voltage: at the same cell voltage, the electron lifetime is significantly larger for the I^-/I_3^- cells. Note that the potential scale is different for the two redox couples, as the counter electrode potential is equal to the respective redox potential; correction for this difference results in a recombination rate that is several orders of magnitude larger for the $[Co(bpy)_3]^{2+/3+}$ redox couple, which is in line with expectations for this one-electron redox couple, as opposed to the much more complex reactions taking place for the I^-/I_3^- redox couple. These results imply that the combination of the OD-8 dye and CDCA does not achieve complete passivation of the ZnO surface, allowing recombination corresponding to electron transfer from the ZnO to the $[Co(bpy)_3]^{2+/3+}$ redox couple. Note that without the CDCA treatment, recombination is even faster for the $[Co(bpy)_3]^{2+/3+}$ redox couple, illustrating the importance of effective surface passivation for ZnO-based DSSCs.

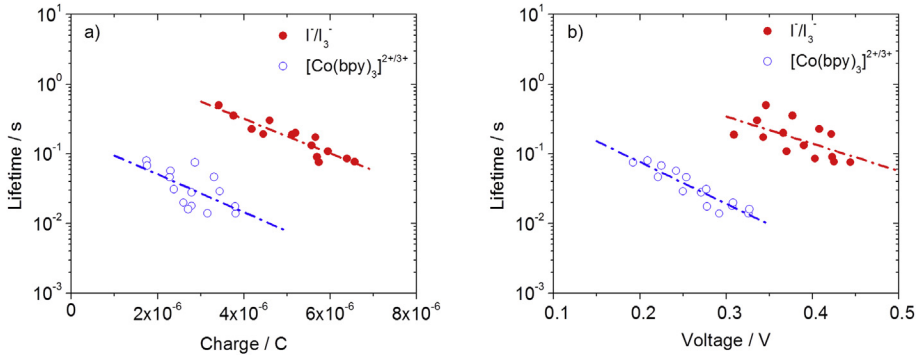

Fig. 8. Electron lifetime as a function of a) the amount of charge extracted, and b) the open-circuit potential (through varying the light intensity). The data presented was obtained for three cells with each redox couple.

4. Conclusions

We have evaluated the performance of dye-sensitized solar cells based on electrodeposited nanostructured, mesoporous ZnO films sensitized with the organic OD-8 dye, in combination with two types of redox couple: the one-electron couple $[Co(bpy)_3]^{2+/3+}$ and the two-electron couple I^-/I_3^-. Electrochemical characterization of the two redox couples illustrate that the redox potential of the $[Co(bpy)_3]^{2+/3+}$ couple is about 0.18 V more positive than that of the I^-/I_3^- couple, however, a corresponding increase in the solar cell open circuit potential is not achieved. Steady-state current-voltage measurements as a function of the immersion time in the dye solutions shows a decrease in performance after a sensitization time of approximately 4 h, and results from scanning electron microscopy and surface photovoltage spectroscopy show that this is likely related to the formation of Zn^{2+}-dye aggregates in the pores of the ZnO film, lowering the injection efficiency and thus the short circuit current density. Combining the results from electron lifetime measurements and open circuit charge extraction measurements leads to the conclusion that the dominant recombination process is electron transfer from ZnO to the oxidized redox agent. Since the electron transfer kinetics to the one-electron $[Co(bpy)_3]^{2+/3+}$ redox couple are much faster, the thermodynamically achievable open circuit potential cannot be sustained thus limiting the performance of the ZnO-OD-8-$[Co(bpy)_3]^{2+/3+}$ solar cell. Based on these results, it is concluded that higher efficiencies should be attainable if an effective ZnO surface passivation method achieving slower electron transfer at the semiconductor/electrolyte interface can be implemented.

Acknowledgements

This material is based upon work supported by a grant from the University of California Institute for Mexico and the United States (UC MEXUS) and the Consejo Nacional de Ciencia y Tecnología de México (CONACYT). M.R.P. gratefully acknowledges CONACYT for a postdoctoral fellowship. The authors also acknowledge CONACYT, SENER and IER-UNAM for funding through the Mexican Center for Innovation in Solar Energy (CeMIE-Sol), Project P-27. F.E.O acknowledges funding by the Department of Energy under DE-SC0015329. We would like to thank Beatriz Heredia Cervera, Leny Pinzón Espinosa, Dora Huerta, and Daniel Aguilar for technical assistance.

Appendix A. Supplementary data

Supplementary data related to this article can be found at https://doi.org/10.1016/j.electacta.2017.11.075.

References

[1] B. O'Regan, M. Grätzel, A low-cost, high-efficiency solar cell based on dye-sensitized colloidal TiO_2 films, Nature 353 (1991) 737–740, https://doi.org/10.1038/353737a0.
[2] M.K. Nazeeruddin, P. Péchy, T. Renouard, S.M. Zakeeruddin, R. Humphry-Baker, P. Cointe, P. Liska, L. Cevey, E. Costa, V. Shklover, L. Spiccia, G.B. Deacon, C.A. Bignozzi, M. Grätzel, Engineering of efficient panchromatic sensitizers for nanocrystalline TiO_2-based solar cells, J. Am. Chem. Soc. 123 (2001) 1613–1624, https://doi.org/10.1021/ja003299u.
[3] Y. Chiba, A. Islam, Y. Watanabe, R. Komiya, N. Koide, L. Han, Dye-sensitized solar cells with conversion efficiency of 11.1%, Jpn. J. Appl. Phys. 45 (2006) L638–L640, https://doi.org/10.1143/JJAP.45.L638.
[4] G. Oskam, B.V. Bergeron, G.J. Meyer, P.C. Searson, Pseudohalogens for dye-sensitized TiO_2 photoelectrochemical cells, J. Phys. Chem. B 105 (2001) 6867–6873, https://doi.org/10.1021/jp004411d.
[5] S.M. Feldt, E.A. Gibson, E. Gabrielsson, L. Sun, G. Boschloo, A. Hagfeldt, Design of organic dyes and cobalt polypyridine redox mediators for high-efficiency dye-sensitized solar cells, J. Am. Chem. Soc. 132 (2010) 16714–16724, https://doi.org/10.1021/ja1088869.
[6] S. Mathew, A. Yella, P. Gao, R. Humphry-Baker, B.F.E. Curchod, N. Ashari-Astani, I. Tavernelli, U. Rothlisberger, M.K. Nazeeruddin, M. Grätzel, Dye-sensitized solar cells with 13% efficiency achieved through the molecular engineering of porphyrin sensitizers, Nat. Chem. 6 (2014) 242–247, https://doi.org/10.1038/nchem.1861.
[7] A. Yella, H.-W. Lee, H.N. Tsao, C. Yi, A.K. Chandiran, M.K. Nazeeruddin, E.W.-G. Diau, C.-Y. Yeh, S.M. Zakeeruddin, M. Graetzel, Porphyrin-sensitized solar cells with cobalt (II/III)-based redox electrolyte exceed 12 percent efficiency, Science 334 (2011) 629–634, https://doi.org/10.1126/science.1209688.
[8] K. Kakiage, Y. Aoyama, T. Yano, K. Oya, J. Fujisawa, M. Hanaya, Highly-efficient dye-sensitized solar cells with collaborative sensitization by silyl-anchor and carboxy-anchor dyes Highly-efficient dye-sensitized solar cells with collaborative sensitization by silyl-anchor and carboxy-anchor dyes, Chem. Commun. 51 (2015) 15894–15897, https://doi.org/10.1039/c5cc06759f.
[9] T.W. Hamann, R.A. Jensen, A.B.F. Martinson, H. Van Ryswyk, J.T. Hupp, Advancing beyond current generation dye-sensitized solar cells, Energy Environ. Sci. 1 (2008) 66, https://doi.org/10.1039/b809672d.
[10] P. Gao, H.N. Tsao, C. Yi, M. Grätzel, M.K. Nazeeruddin, Extended π-bridge in organic dye-sensitized solar cells: the longer, the better? Adv. Energy Mater. 4 (2014) 1301485, https://doi.org/10.1002/aenm.201301485.
[11] N.M. Gómez-Ortíz, J. Idígoras, E. Guillén, A. Hernández, A. Sastre-Santos, F. Fernández-Lázaro, J.A. Anta, G. Oskam, Influence of dye chemistry and electrolyte solution on interfacial processes at nanostructured ZnO in dye-sensitized solar cells, J. Photochem. Photobiol. A Chem. 264 (2013) 26–33, https://doi.org/10.1016/j.jphotochem.2013.04.020.
[12] L.M. Peter, Characterization and modeling of dye-sensitized solar cells, J. Phys. Chem. C 111 (2007) 6601–6612, https://doi.org/10.1021/jp069058b.
[13] Q. Zhang, C.S. Dandeneau, X. Zhou, G. Cao, ZnO nanostructures for dye-sensitized solar cells, Adv. Mater. 21 (2009) 4087–4108, https://doi.org/10.1002/adma.200803827.
[14] Y. Natsume, H. Sakata, Zinc oxide films prepared by sol-gel spin-coating, Thin Solid Films 372 (2000) 30–36, https://doi.org/10.1016/S0040-6090(00)01056-7.
[15] J.-H. Lee, K.-H. Ko, B.-O. Park, Electrical and optical properties of ZnO transparent conducting films by the sol–gel method, J. Cryst. Growth 247 (2003) 119–125, https://doi.org/10.1016/S0022-0248(02)01907-3.
[16] H.R. Ghorbani, F.P. Mehr, H. Pazoki, B.M. Rahmani, Synthesis of ZnO nanoparticles by precipitation method, Orient. J. Chem. 31 (2015) 1219–1221.
[17] D. Raoufi, Synthesis and microstructural properties of ZnO nanoparticles prepared by precipitation method, Renew. Energy 50 (2013) 932–937, https://doi.org/10.1016/j.renene.2012.08.076.
[18] R.K. Sharma, R. Ghose, Synthesis of zinc oxide nanoparticles by homogeneous precipitation method and its application in antifungal activity against Candida

albicans, Ceram. Int. 41 (2015) 967–975, https://doi.org/10.1016/j.ceramint.2014.09.016.
[19] P. Pandey, R. Kurchania, F.Z. Haque, Controlled hydrothermal synthesis, structural and optical analysis of nanometer-sized ZnO spheres, Optik 126 (2015) 301–303, https://doi.org/10.1016/j.ijleo.2014.08.160.
[20] J. Yu, X. Yu, Hydrothermal synthesis and photocatalytic activity of zinc oxide hollow spheres, Environ. Sci. Technol. 42 (2008) 4902–4907, https://doi.org/10.1021/es800036n.
[21] Z. Chen, Y. Tang, L. Zhang, L. Luo, Electrodeposited nanoporous ZnO films exhibiting enhanced performance in dye-sensitized solar cells, Electrochimica Acta 51 (2006) 5870–5875, https://doi.org/10.1016/j.electacta.2006.03.026.
[22] F.I. Lizama Tzec, M.A. Aguilar Frutis, G. Rodríguez Gattorno, G. Oskam, Electrodeposition of ZnO for application in dye-sensitized solar cells, J. New Mater. Electrochem. Syst. 16 (2013) 209–215.
[23] B. Canava, D. Lincot, Nucleation effects on structural and optical properties of electrodeposited zinc oxide on tin oxide, J. Appl. Electrochem. 30 (2000) 711–716, https://doi.org/10.1023/A:1003857026200.
[24] A.I. Inamdar, S.H. Mujawar, S.R. Barman, P.N. Bhosale, P.S. Patil, The effect of bath temperature on the electrodeposition of zinc oxide thin films via an acetate medium, Semicond. Sci. Technol. 23 (2008) 85013, https://doi.org/10.1088/0268-1242/23/8/085013.
[25] L.H. Mendoza-Huízar, C.H. Rios-Reyes, M.G. Gómez-Villegas, Zinc electrodeposition from chloride solutions onto glassy carbon electrode, J. Mexican Chem. Soc. 53 (2009) 243–247.
[26] T. Yoshida, D. Komatsu, N. Shimokawa, H. Minoura, Mechanism of cathodic electrodeposition of zinc oxide thin films from aqueous zinc nitrate baths, Thin Solid Films 451–452 (2004) 166–169, https://doi.org/10.1016/j.tsf.2003.10.097.
[27] O. Lupan, V.M. Guérin, I.M. Tiginyanu, V.V. Ursaki, L. Chow, H. Heinrich, T. Pauporté, Well-aligned arrays of vertically oriented ZnO nanowires electrodeposited on ITO-coated glass and their integration in dye sensitized solar cells, J. Photochem. Photobiol. A Chem. 211 (2010) 65–73, https://doi.org/10.1016/j.jphotochem.2010.02.004.
[28] T. Yoshida, K. Terada, Electrochemical self assembly of nanoporous ZnO/eosin Y thin films and their sensitized photoelectrochemical performance, Adv. Mater. 2 (2000) 1214–1217, https://doi.org/10.1002/1521-4095(200008)12:16<1214::AID-ADMA1214>3.0.CO;2-Z.
[29] R. Tena-Zaera, J. Elias, G. Wang, C. Lévy-Clément, Role of chloride ions on electrochemical deposition of ZnO nanowire arrays from O_2 reduction, J. Phys. Chem. C 111 (2007) 16706–16711, https://doi.org/10.1021/jp073985g.
[30] Y. He, J. Hu, Y. Xie, High-efficiency dye-sensitized solar cells of up to 8.03% by air plasma treatment of ZnO nanostructures, Chem. Commun. 51 (2015) 16229–16232, https://doi.org/10.1039/c5cc04567c.
[31] J. Idígoras, G. Burdziński, J. Karolczak, J. Kubicki, G. Oskam, J.A. Anta, M. Ziółek, The impact of the electrical nature of the metal oxide on the performance in dye-sensitized solar cells: new look at old paradigms, J. Phys. Chem. C 119 (2015) 3931–3944, https://doi.org/10.1021/jp512330f.
[32] J.A. Anta, E. Guillén, R. Tena-Zaera, ZnO-based dye-sensitized solar cells, J. Phys. Chem. C 116 (2012) 11413–11425, https://doi.org/10.1021/jp3010025.
[33] S. Peulon, Mechanistic study of cathodic electrodeposition of zinc oxide and zinc hydroxychloride films from oxygenated aqueous zinc chloride solutions, J. Electrochem. Soc. 145 (1998) 864, https://doi.org/10.1149/1.1838359.
[34] H. Nusbaumer, J.-E. Moser, S.M. Zakeeruddin, M.K. Nazeeruddin, M. Grätzel, $Co^{II}(dbbip)_2^{2+}$ complex rivals tri-iodide/iodide redox mediator in dye-sensitized photovoltaic cells, J. Phys. Chem. B 105 (2001) 10461–10464, https://doi.org/10.1021/jp012075a.
[35] H. Nusbaumer, S.M. Zakeeruddin, J.-E. Moser, M. Grätzel, An alternative efficient redox couple for the dye-sensitized solar cell system, Chem. A Eur. J. 9 (2003) 3756–3763, https://doi.org/10.1002/chem.200204577.
[36] J.-H. Yum, E. Baranoff, F. Kessler, T. Moehl, S. Ahmad, T. Bessho, A. Marchioro, E. Ghadiri, J.-E. Moser, C. Yi, M.K. Nazeeruddin, M. Grätzel, A cobalt complex redox shuttle for dye-sensitized solar cells with high open-circuit potentials, Nat. Commun. 3 (2012) 631–639, https://doi.org/10.1038/ncomms1655.
[37] H. Shahroosvand, P. Abbasi, M. Ameri, M. Riahi, Dye-sensitized nanocrystalline ZnO solar cells based on ruthenium(II) phendione complexes, Int. J. Photoenergy 2011 (2011), https://doi.org/10.1155/2011/634147.
[38] I. Gonzalez-Valls, M. Lira-Cantu, Dye sensitized solar cells based on vertically-aligned ZnO nanorods: effect of UV light on power conversion efficiency and lifetime, Energy Environ. Sci. 3 (2010) 789, https://doi.org/10.1039/b922354a.
[39] H. Horiuchi, R. Katoh, K. Hara, M. Yanagida, S. Murata, H. Arakawa, M. Tachiya, Electron injection efficiency from excited N3 into nanocrystalline ZnO films: effect of ($N3–Zn^{2+}$) aggregate formation, J. Phys. Chem. B 107 (2003) 2570–2574, https://doi.org/10.1021/jp0220027.
[40] W.-C. Chang, C.-H. Lee, W.-C. Yu, C.-M. Lin, Optimization of dye adsorption time and film thickness for efficient ZnO dye-sensitized solar cells with high at-rest stability, Nanoscale Res. Lett. 7 (2012) 688, https://doi.org/10.1186/1556-276X-7-688.
[41] J.A. Anta, J. Idigoras, E. Guillen, J. Villanueva-Cab, H.J. Mandujano-Ramirez, G. Oskam, L. Pelleja, E. Palomares, A continuity equation for the simulation of the current-voltage curve and the time-dependent properties of dye-sensitized solar cells, Phys. Chem. Chem. Phys. 14 (2012) 10285–10299, https://doi.org/10.1039/c2cp40719a.
[42] P.R.F. Barnes, K. Miettunen, X. Li, A.Y. Anderson, T. Bessho, M. Graetzel, B.C. O'Regan, Interpretation of optoelectronic transient and charge extraction measurements in dye-sensitized solar cells, Adv. Mater. 25 (2013) 1881–1922, https://doi.org/10.1002/adma.201201372.